Macromolecules
ARTICLE

Macromolecules **2009**, *42*, 9089–9095 **9089**
DOI: 10.1021/ma9017263

Thermodynamics of Polymer−Clay Nanocomposites Revisited: Compressible Self-Consistent Field Theory Modeling of Melt-Intercalated Organoclays

Valeriy V. Ginzburg,*,† Jeffrey D. Weinhold,‡ Prasanna K. Jog,† and Rakesh Srivastava†

†*Corporate Research and Development, The Dow Chemical Company, Midland, Michigan 48674, and*
‡*Corporate Research and Development, The Dow Chemical Company, Freeport, Texas 77515*

Received August 3, 2009; Revised Manuscript Received October 16, 2009

ABSTRACT: We formulate a "compressible" version of lattice self-consistent field theory (SCFT) to describe thermodynamic behavior of organically modified clays in polymer melt. The melt consists of the homopolymer matrix and a fraction of end-functionalized "active" chains, each chain having a single "sticker" end-group with strong affinity to the clay surface. We calculate the phase map for this system as a function of the melt composition and the strength of the "sticker" adhesion to the clay. It is shown that within the compressible SCFT model intercalated morphologies are favored in a significantly broader parameter range than was expected based on the incompressible SCFT analysis. We provide a qualitative analysis of this result and discuss implications for the physics of nanocomposites in general.

Introduction

Polymer−clay nanocomposites have attained substantial interest in the past two decades, since the successful development of a nylon-6/montmorillonite hybrid by Okada et al. at Toyota research laboratories.[1] Since then, hybrid polymer−clay nanocomposites were successfully prepared using polyethylene (PE), polypropylene (PP), poly(methyl methacrylate) (PMMA), polystyrene (PS), epoxy, polyurethane, and other matrices (see, e.g., review articles by Sinha Ray and Okamoto[2] and Alexandre and Dubois[3]). It has been shown that under some conditions such nanocomposite materials could provide 2−4 times increase in the elastic modulus, order of magnitude decrease in gas permeability, and substantial reduction of flammability compared to the pristine polymer matrix, at clay loadings of less than 10 wt %. However, it was also recognized early on that the property enhancement, if any, depends strongly on the morphology of the nanocomposite and the quality of nanoclay dispersion in the matrix. In many cases, clay platelets fail to disperse and remain aggregated into large (micrometer-sized) "stacks"; in this case, modulus and strength of the composite could be comparable to those of the matrix polymer, while, e.g., toughness and ultimate elongation could even worsen. Therefore, the ability to disperse nanoclays on a molecular level has been recognized early on as the critical problem in nanocomposite science and technology.

Nanoclay dispersion on a molecular level (often referred to as exfoliation, see Figure 1a) generally depends on a variety of factors, both "thermodynamic" and "dynamic". The former include various contributions (van der Waals, electrostatic, and polymer-induced) to the effective clay−clay interactions; the latter describe processing history and effective forces applied to break up the original clay stacks. While dynamic factors are crucial in breaking up the original stacks, thermodynamic factors are of utmost importance in ensuring that the platelets would stay apart and not reagglomerate once shear is removed; because of this, most recent theoretical effort has been concentrated on thermodynamics. Thus, Vaia and Giannelis[4,5] addressed the issue of nanocomposite morphology by considering the interaction of organically modified silicates (OLS) with a homopolymer melt. They developed a lattice mean-field model that calculated both enthalpic and entropic contributions to the free energy of short grafted chains and longer matrix polymers in the gallery between two adjacent clay platelets (Figure 1b). Vaia and Giannelis demonstrated that as the organoclay platelets attempt to separate, there needs to be a flow of polymer into the gallery, resulting in the substantial loss of entropy for the newly confined chains. This loss of entropy could be compensated by enthalpic gain, provided that the interaction between the polymer and the clay platelet is favorable. Thus, formation of exfoliated nanocomposites is easier in more polar polymers (nylon-6, epoxy) than in less polar ones (polyethylene, polypropylene). As one varies the balance between enthalpic and entropic interactions, various types of free energy profiles $F(H)$ can be obtained (Figure 1c); here, F is the polymer-related free energy per unit area of the clay platelet, and H is the separation between the platelets (often referred to as gallery height). If F is monotonically increasing function of H, the composite is likely to be "immiscible"; if $F(H)$ is monotonically decreasing, exfoliated morphology is favored; finally, if there is a minimum at a finite separation H^*, it points to intercalated morphology with most probable gallery height equal to H^*.

The approach of Vaia and Giannelis was subsequently extended by Balazs and co-workers. In a series of papers, Balazs et al.[6−12] successfully applied lattice self-consistent field theory (SCFT) formalism of Scheutjens and Fleer[13−15] to calculate polymer-mediated clay−clay interaction for several cases: organically modified clays in a homopolymer melt, organically modified clays in the melt with some end-functionalized ("one-sticker") chains, and organically modified clays in the melt of telechelic ("two-sticker") chains. In addition to the lattice SCFT analysis, Balazs and co-workers also utilized strong segregation theory[6,7,11,12] to investigate the influence of different configurations of adsorbed chains (loops, bridges, and trains). In addition, Balazs et al.[9,10,16,17] utilized anisotropic colloid models to

*Author for correspondence. E-mail: vvginzburg@dow.com.

Published on Web 10/26/2009

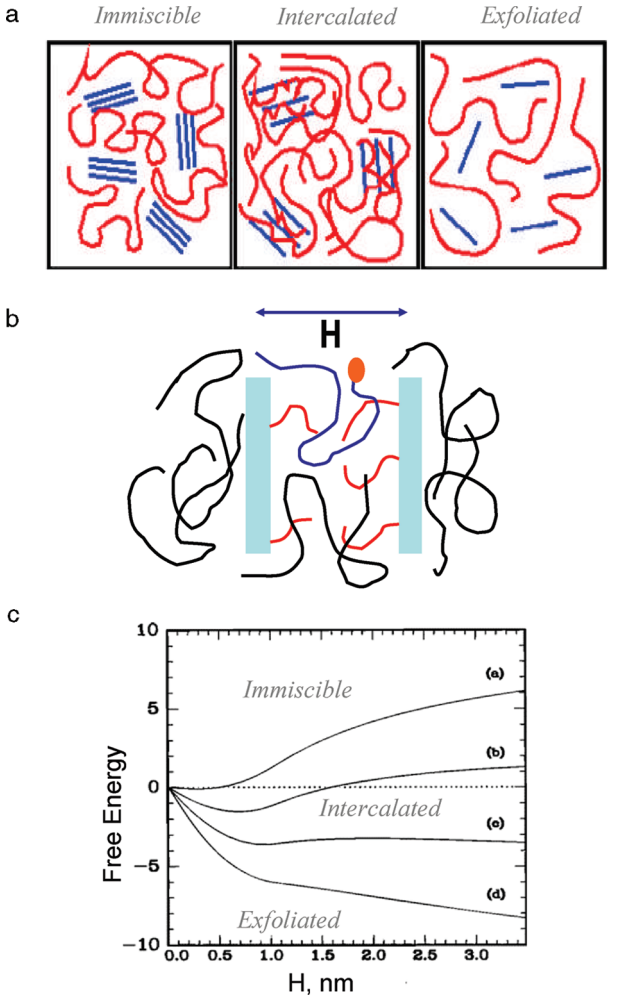

Figure 1. (a) Idealized representation of nanocomposite morphologies. (b) Schematic depiction of the gallery between two adjacent platelets, with grafted chains (red), free chains (black), and end-functionalized chains (blue). (c) Representative free energy curves corresponding to different morphologies (after Vaia and Giannelis[4]).

describe the dependence of the phase behavior of the nanoclay aspect ratio and volume fraction. In particular, in a practically important case of organically modified clays in a homopolymer melt, it was shown that clay platelets could favor aggregation even when there is no enthalpic repulsion between the matrix polymer and the surfactant (Flory−Huggins parameter $\chi_{PS} = 0$), provided that the surfactant has low chain length and high grafting density. This prediction was indeed confirmed for cases like the mixtures of montmorillonite clay with C16 or C18 grafted chains, melt compounded with polyethylene or polypropylene; such systems were demonstrated to be mostly immiscible, in agreement with theoretical predictions.[2,18,19] Similarly, for the cases where end-functionalized chains (e.g., maleated polypropylene) were added to the melt, intercalated and exfoliated morphologies could be observed,[2,20−23] as predicted by the theory.

In our view, one area where predictions of the lattice SCFT are not fully satisfactory is in predicting intercalated morphologies. Indeed, there are numerous nanocomposite systems exhibiting intercalated morphology with a typical gallery spacing $H^* \sim 1$—2 nm (10—20 Å). While lattice SCFT does predict intercalated morphologies in various systems,[6−8] the gallery spacing corresponding to those structures is expected to be somewhat larger than observed (probably on the order of 4—10 nm, depending on the molecular weight of the functionalized chains). Furthermore, in recent experimental studies by Swain and Isayev,[24] intercalated structures have been reported even in systems without "stickers" (Cloisite 20A in high-density polyethylene) when they were subjected to strong ultrasound treatment in the melt state. The increase in the clay−clay spacing (compared to the pure organoclay), measured by wide-angle X-ray scattering (WAXS), was fairly small (from 2.4 to 3.56 nm). In a sense, it appears that intercalated structures are far more ubiquitous than originally predicted by the theory.

What could be the origin of the large number of intercalated structures in polymer−clay composites? Usually, if an intercalated morphology is observed in systems where expected morphology is exfoliated or immiscible, two explanations are suggested: (i) intercalated morphology is the result of the interplay between the polymer-induced interaction and direct clay−clay interaction (electrostatic and van der Waals), or (ii) intercalated morphology is not thermodynamically stable, but a "kinetically trapped" or metastable one. While not disputing these explanations—which probably hold true in many instances—we intend to demonstrate that intercalated morphologies can also naturally appear as equilibrium or metastable states when only the polymer-mediated free energy is evaluated. The proper mechanism for this is accounting for compressibility (density variation) in the gallery, as discussed below.

Recently, we utilized the interfacial statistical associating fluid theory (iSAFT) formalism of the polymer density functional theory (DFT) to study the interaction between polymer brushes immersed in a polymer melt.[25] Within a DFT, one could prescribe a bulk polymer density (or "packing fraction") and calculate the equilibrium polymer density profiles within the gallery as a function of the gallery height and spatial location. One can also evaluate free energy or normal force acting between the platelets to which the brushes are grafted. We found that the behavior of the system was, under some conditions, a strong function of the bulk packing fraction—at very high packing fractions (> 0.75), polymer interactions favored exfoliation, while at lower packing fractions (~0.4−0.6), there was a minimum at some finite gallery height H^*, indicating the preference toward intercalated structures. Motivated by this discovery, we employed a slightly modified lattice SCFT formalism in which compressibility was introduced by adding "voids" acting as solvents (thus, equations of our SCFT were similar to those of van Lent et al.,[26] who studied the behavior of grafted chains in concentrated polymer solutions). We found that within this "compressible" SCFT one can observe the same trends as predicted using iSAFT; indeed, the two theories showed remarkable agreement for the intermediate-to-high bulk polymer packing fractions (0.6−0.75). In this model, when the gallery height is very small, the density inside the gallery is higher than in the bulk, and there is a strong pressure pushing the platelets apart. At the point when the densities inside and outside become approximately equal, the free energy reaches its effective minimum. Further expansion is unfavorable for obvious reasons: bulk polymer chains moving to the gallery would suffer entropy losses, while further addition of voids would make the density in the gallery substantially lower than in the bulk.

The results of the above study were restricted to "athermal" case (all Flory−Huggins parameters, $\chi_{ij} = 0$). In general, however, even if organic modifiers and bulk chains have the same chemistry (e.g., when the matrix polymers are polyolefins like PE or PP), the void−polymer interaction parameter must be nonzero (otherwise, polymer would have had a near-zero surface tension). In addition, in many cases, exfoliation promoters such as one- or multisticker chains are used, and it would be important to apply our new modeling formalism to those systems. Such an analysis is

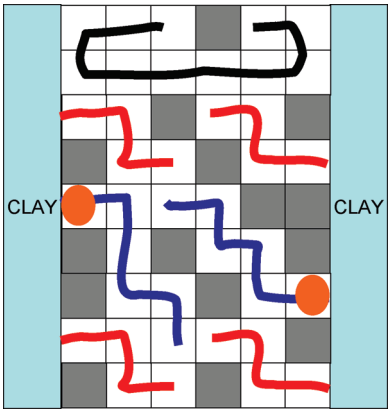

Figure 2. Schematic depiction of the lattice model. Note that some of the lattice sites are not occupied by polymeric species—those are "voids".

the topic of this paper. We first describe the "compressible" lattice SCFT formalism; next, we investigate the phase maps for ternary systems consisting of organoclays, homopolymers, and one-sticker end-functionalized chains. The paper is concluded by discussion of the essential physics of intercalation and proposed next steps in the theoretical analysis.

The Model

Our lattice model is schematically depicted in Figure 2. In its most general form, the grand canonical free energy per unit area, f, is written as

$$f = \frac{G}{Ma^2 k_B T} = \sigma \ln\left(\frac{\sigma N_g}{\sum_{z=1}^{H} G_g(z, N_g)}\right) + \sum_i \frac{\Theta_i}{N_i} \ln \varphi_i^b + \Theta_v \ln \varphi_v^b - \sum_i \mu_i \frac{\Theta_i}{N_i} - \mu_v \Theta_v + \frac{1}{2}\left(\sum_{z=1}^{H}\left(\sum_{\alpha,\beta} \chi_{\alpha\beta}(\phi_\alpha(z) - \phi_\alpha^b)\left(\langle\phi_\beta(z)\rangle - \phi_\beta^b\right)\right)\right) - \sum_{z=1}^{H}\left(\sum_\alpha u_\alpha(z)\phi_\alpha(z)\right) \quad (1)$$

Here, a is the lattice unit dimension, M is the number of lattice units per clay platelet (so that the product $Ma^2 = A$ is the total area of the platelet), σ is the grafting density of "surfactants", $\chi_{\alpha\beta}$ are the Flory−Huggins parameters between species α and β, μ_i is the chemical potential of the ith component, and Θ_i is the excess amount of the ith component in the system. The density profiles of various species, $\phi_\alpha(z)$, and conjugate fields, $u_\alpha(z)$, are calculated as described below. Note that we introduce a separate species and component—voids (denoted as subscript v)—to account for density variation within the gallery.

The bulk chemical potentials of all polymers and voids are described as

$$\mu_i = ln\, \varphi_i^b + (1 - N_i)(1 - \varphi_i^b) \quad (2a)$$

$$\mu_v = ln\, \varphi_v^b + \sum_i \frac{\varphi_i^b}{N_i}(1 - N_i) \quad (2b)$$

In eqs 1 and 2, densities with superscript b refer to the equilibrium densities in the bulk (for all components and all species). The excess amount of each component, Θ, is given by

$$\Theta_i = \sum_{z=1}^{H} \phi_i(z) \quad (3a)$$

$$\Theta_v = \sum_{z=1}^{H} \phi_v(z) \quad (3b)$$

The effective fields, $u_\alpha(z)$ and $u_v(z)$, are given by

$$u_\alpha(z) = u'(z) + \frac{1}{2}\sum_\beta \chi_{\alpha\beta}\{\langle\phi_\alpha(z)\rangle - \varphi_\alpha^b\} \quad (4a)$$

$$u_v(z) = u'(z) + \frac{1}{2}\sum_\beta \chi_{\beta v}\{\langle\phi_\beta(z)\rangle - \varphi_\beta^b\} \quad (4b)$$

The effective hard core potential $u'(z)$ is a Lagrange multiplier that enforces the incompressibility condition:

$$\sum_\alpha \phi_\alpha(z) + \phi_v(z) + \phi_g(z) = 1 \quad (5)$$

To complete the set of equations needed to calculate the free energy and density profiles, one needs the rules to evaluate density profiles. The local density of the voids, $\phi_v(z)$, is calculated always from eq 5, while the calculation of the density of the polymeric components is more complicated and depends on the specific composition of the bulk polymer and the architecture of each polymeric component. We restrict ourselves to the systems in which the bulk contains two types of polymer: "free" or "matrix" homopolymer chains and "active" or "end-functionalized" chains with one "sticker". For each type of chain (including the grafted surfactants), one can evaluate the "propagators" $G(z,s)$ and $G^*(z,s)$. (The propagators are evaluated assuming Markov statistical process for Gaussian chains occupying various lattice sites.) All the propagators obey the same recurrence equation:

$$Y(z, s) = \langle Y(z, s-1)\rangle G_{t(s)}(z) \quad (6)$$

Here, Y is a shorthand for one of the five propagators: $G_g(z,s)$ and $G_g^*(z,s)$ (for grafted chains), $G_a(z,s)$ and $G_a^*(z,s)$ (for "active" chains), and $G_f(z,s)$ (for "free" chains; due to symmetry, $G^*_f(z,s) = G_f(z,s)$). The factor $G_\alpha(z)$ is the Boltzmann factor for the specie of type α to be at position z compared to the bulk:

$$G_\alpha(z) = \exp(-u_\alpha(z)) \quad (7)$$

In eq 6, index $t(s)$ labels the specie type of a monomer having position s in the chain. For the case of "free" chains, all monomers are the same (we label them as "F"):

$$\phi_F(z) = \sum_{s=1}^{N_f}\left(\frac{\varphi_f^b}{N_f}\right)\frac{G_f(z,s)G_f(z, N_f - s + 1)}{G_F(z)} \quad (8a)$$

For the grafted chains, all monomers are also the same (we label them as "G"):

$$\phi_G(z) = \sum_{s=1}^{N_g}\left(\frac{\sigma}{\sum_{z'=1}^{H} G_g(z', N_g)}\right)\frac{G_g(z,s)G_g^*(z, N_g - s + 1)}{G_G(z)} \quad (8b)$$

Finally, for active chains, there are two types of monomers: "sticker" (at position $s = 1$) and the rest (positions $s = 2$ to N_a),

labeled as "*S*" and "*A*", respectively:

$$\phi_S(z) = \sum_{s=1}^{1} \left(\frac{\varphi_a^b}{N_a}\right) \frac{G_a(z,s)G_a(z,N_a - s + 1)}{G_S(z)} \quad (8c)$$

$$\phi_A(z) = \sum_{s=2}^{N_a} \left(\frac{\varphi_a^b}{N_a}\right) \frac{G_a(z,s)G_a(z,N_a - s + 1)}{G_A(z)} \quad (8d)$$

In eqs 1, 4a4, and 6, $\langle ... \rangle$ denotes local averaging according to the prescription

$$\langle Y(z) \rangle = \lambda_{-1} Y(z-1) + \lambda_0 Y(z) + \lambda_1 Y(z+1) \quad (9)$$

Constants λ_{-1}, λ_0, and λ_1 are determined by the choice of the lattice; in our calculations, $\lambda_{-1} = \lambda_1 = 0.25$, $\lambda_0 = 0.5$. This choice corresponds to the simple cubic lattice which is commonly used in the application of lattice SCFT to polymer−clay composites. To relate the lattice coordinate to "real" dimensions, we must also specify the value of the lattice size a; here, we set $a = 0.4$ nm. (In the following text, we will automatically convert all results from lattice units to nanometers.)

Recursive relation 7 must be solved for $s = 1$ to N_f for the free chain propagator $G_f(z,s)$, for $s = 1$ to N_g for the grafted chain related propagators $G_g(z,s)$ and $G_g^*(z,s)$, and for $s = 1$ to N_a for the active chain propagators $G_a(z,s)$ and $G_a^*(z,s)$. The initial conditions are as follows: $G_f(z,1) = G_F(z)$, $G_g(z,1) = G_G(z)\delta_{z1}$, $G_g^*(z,1) = G_G(z)$, $G_a(z,1) = G_S(z)$, and $G_a^*(z,1) = G_A(z)$.

Equations 1−9 are solved on a lattice in an iterative fashion until a convergence criterion (e.g., the difference between free energy calculations from the two successive iterations) is satisfied.

We now move to describe the application of this model to the prediction of the phase diagrams of polymer−clay composites.

Results and Discussion

We consider model system in which bulk polymer consists of "free" matrix chains ($N_f = 300$) and "active" one-sticker chains ($N_a = 100$). Flory−Huggins interaction parameters between various species are summarized in Table 1. This corresponds to the scenario in which surfactants, matrix chains, and functionalized chains are all hydrocarbon molecules (for example, surfactant is a C12 linear chain, matrix is a 100 000 molecular weight polyethylene, and functionalized chain is a shorter polyethylene molecule with one grafted maleic group). The nonzero interaction parameter between voids and hydrocarbon monomers reflects nonzero surface tension of polyethylene.[27,28] The interaction parameter between the clay surface and hydrocarbon monomers $\chi_{\alpha c} = 1.0$ ($\alpha = G, F, A$), reflecting a very strong incompatibility between the nonpolar polymers and the polar clay surface. The interaction parameter between the clay surface and voids—related to the surface tension of the bare clay—was set to 2.0 to reflect the fact that the surface energy of the clay should be much higher than that of the polymers. Finally, the interaction parameter between the stickers and the clay surface, χ_{SC}, was varied to study the influence of the adhesion strength on the phase behavior. (The range of χ_{SC} investigated here, between 0 and −100, roughly corresponds to sticker−surface adhesion energy, $\varepsilon = -\chi_{SC}/6$,[7,10] being bracketed between 0 and 10 kcal/mol, which is typical for hydrogen-bonding interactions.) We also varied the volume (or weight) fraction of the active chains. Finally, all the calculations were repeated for two densities: $\phi_v^b = 0$ (incompressible melt, the model equivalent to earlier studies of Balazs et al.), and $\phi_v^b = 0.4$ (compressible melt). The length of the grafted chains, $N_{gr} = 5$, and the grafting density, $\rho_{gr} = 0.2$, were chosen to match the earlier study of Ginzburg and Balazs.[10] (One difference between the current study and that of ref 10 is that in the earlier study Flory−Huggins parameters between the clay and the polymers were set to zero.)

Table 1. Flory−Huggins Interaction Parameters Used in the Calculations

	G	*F*	*A*	*S*	*V*
grafted (*G*)	0.0	0.0	0.0	0.0	1.0
free matrix (*F*)	0.0	0.0	0.0	0.0	1.0
active (*A*)	0.0	0.0	0.0	0.0	1.0
sticker (*S*)	0.0	0.0	0.0	0.0	1.0
void (*V*)	1.0	1.0	1.0	1.0	0.0

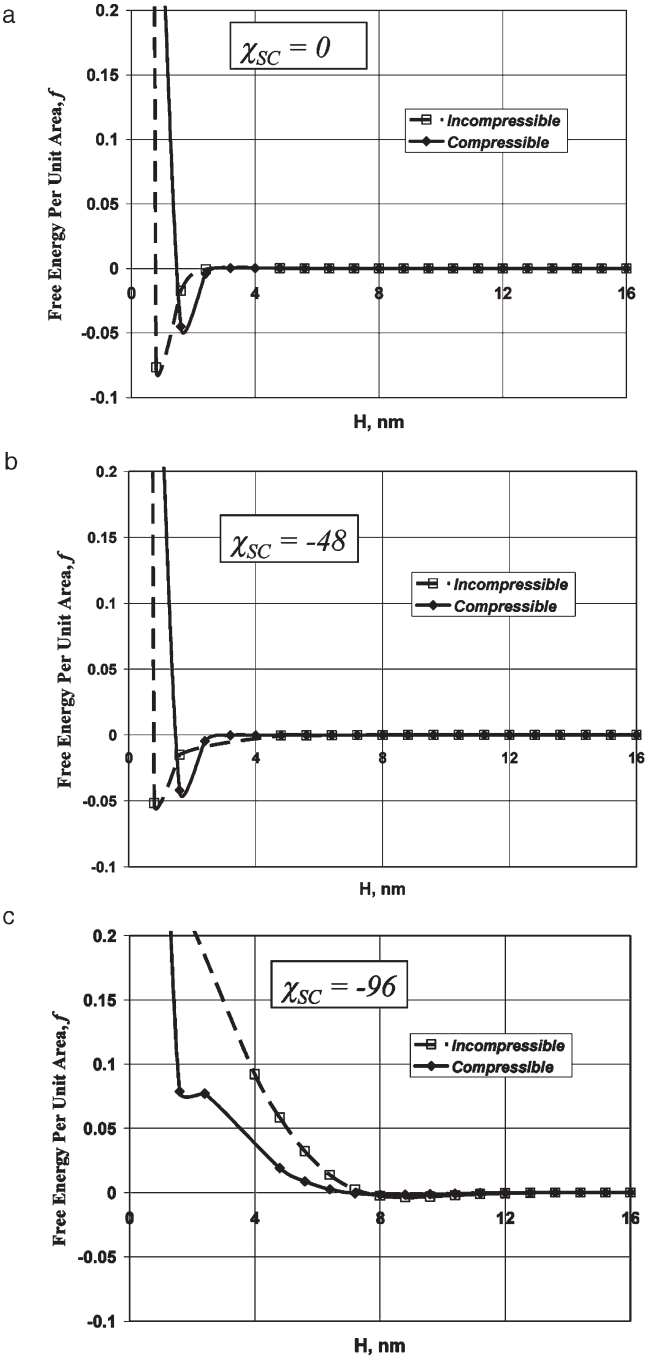

Figure 3. Calculated free energy (per unit area) profiles based on compressible (solid) and incompressible (dashed) lattice SCFT approaches. (a) $\chi_{SC} = 0$; (b) $\chi_{SC} = -48$; (c) $\chi_{SC} = -96$. Free energy per unit area, f, is calculated according to eq 1. For more details, see text.

In Figure 3, we plot calculated free energies, $f(H)$, for several values of χ_{SC}, while keeping the active chain weight fraction

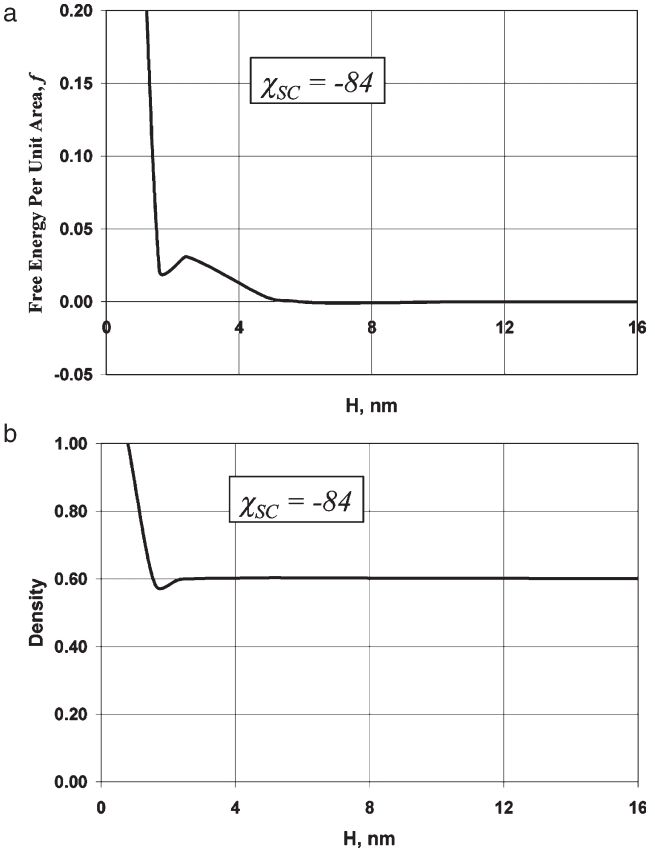

Figure 4. Free energy per unit area (a) and overall polymer density (b) as a function of the gallery height H for the $\chi_{SC} = -84$ system. Calculations are based on the compressible lattice SCFT model.

constant at 0.05 (same as in the study by Ginzburg and Balazs[10]). In all cases, the dashed lines correspond to the incompressible model, and the solid lines are compressible model calculations. We can now carefully examine some of the results.

At low adhesion strength between the sticker and the clay (Figure 3a,b), the free energy has a deep, sharp minimum at small separation. Note that for the incompressible system this minimum corresponds to the gallery which is "completely closed", and thus, the plate separation is the same as for the neat organoclay ("immiscible morphology"). For the compressible system, the gallery opens up slightly (the increase in the gallery height is approximately 0.8−1 nm), and the structure that forms is now likely to be interpreted as "intercalated".

For the system with very high adhesion strength between the clay and the stickers, the favorable enthalpy of the sticker−clay interaction dominates the unfavorable entropic contributions. Accordingly (Figure 3c), the composite now becomes exfoliated, as demonstrated by both compressible and incompressible models. Interestingly, within the compressible model, the old minimum at $H \sim 1.6-2$ nm has not disappeared completely, indicating the presence of a metastable intercalated morphology. (As we already mentioned, polymer-mediated intercalated minimum for the case of two-sticker or telechelic chains was predicted by several authors,[7,11−29] but the mechanism there was bridging intercalation, which is not applicable for the one-sticker chains considered here.)

What is the origin of this minimum? To understand that, we examined in more detail the case of $\chi_{SC} = -84$. Its compressible free energy profile is shown in Figure 4a, once again indicating the presence of a well-defined minimum at small separations. In Figure 4b, we plot the dependence of polymer density (sum of the volume fractions of all components except for voids) in the

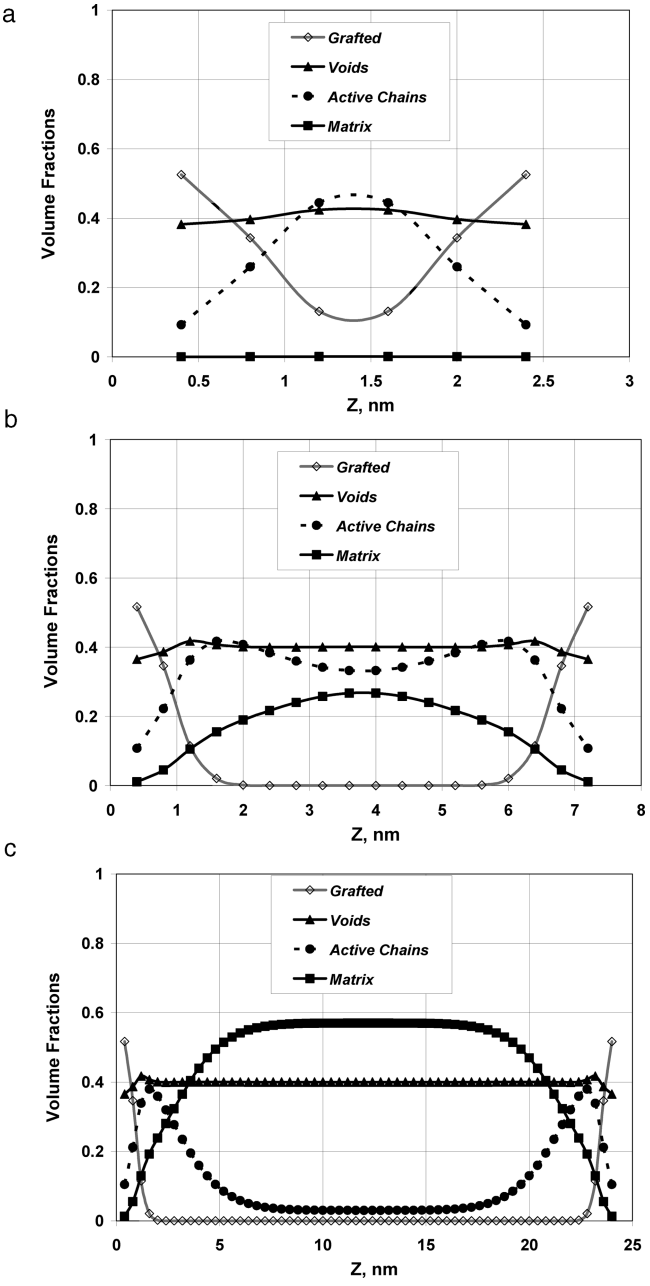

Figure 5. Calculated density profiles for the $\chi_{SC} = -84$ system at various gallery heights H: (a) $H = 2.4$ nm (6 lattice units); (b) $H = 7.2$ nm (18 lattice units); (c) $H = 24$ nm (60 lattice units).

gallery on the gallery height. It can be seen that the free energy minimum coincides with the density minimum. Thus, the voids are the first to intercalate the gallery—this initial expansion simply due to the density reduction inside the gallery takes place even before the sticker attachment. The analysis of density profiles at different gallery heights helps understand this. At small separations (Figure 5a), the gallery is penetrated by some active chains, but their amount is relatively low, while the fraction of voids is slightly larger than in the bulk. The grafted chains form strongly overlapping brushes. At intermediate separations (Figure 5b), the brushes no longer overlap, and some matrix chains begin to penetrate the gallery, although end-functionalized chains still account for the majority of the intragallery polymer. Finally, at large separations (gallery height much greater than radius of gyration of the active chains), the composition in the center of the gallery is close to that of the bulk polymer, while near the surfaces, there is excess of active chains (Figure 5c).

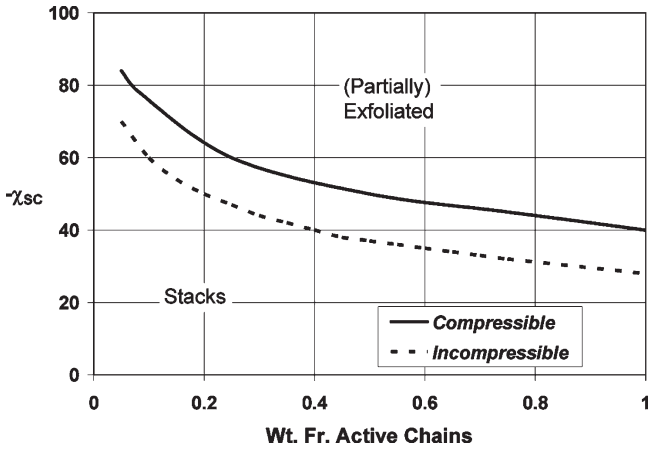

Figure 6. Calculated nanocomposite phase diagram (in the limit of small organoclay loadings). Solid line is the phase boundary between weakly intercalated stacks and partially exfoliated, partially intercalated phase, as calculated using compressible SCFT. Dashed line is the phase boundary between immiscible and exfoliated phases, as calculated by incompressible SCFT.

The discussion above centered on a single active chain weight fraction $x = 5$ wt %. We calculated free energy profiles as a function of χ_{SC} for several polymer compositions, varying active chain content from 0 to 100%. The resulting phase diagram is shown in Figure 6. It can be seen that according to the "compressible" model the range where intercalated structures could be found has dramatically expanded. Basically, the "initial" intercalation occurs when the plates are separated only slightly, and the "voids" enter the gallery, thereby substantially decreasing the density of the grafted surfactant. The amount of active polymer entering the gallery is still relatively low. As the gallery height is increased further, the addition of the active chains requires that density go up, thus resulting in the loss of translational entropy for the "voids". (Alternatively, this could be thought of simply as additional entropic penalty for higher polymer density.) This increase in the free energy could overcome the enthalpic gain from adding a few "stickers" attached to the clay surfaces. Only when the separation is increased substantially, and the number of "stickers" attached to the surface becomes sufficiently high, can free energy decrease to its global minimum.

The above predictions are certainly dependent on the choices of the Flory−Huggins interaction parameters, relative molecular weights of matrix and sticker chains, matrix polymer density, etc. Even so, the main predictions of the "compressible model"—the shifting of the global free energy minimum toward higher H for the "immiscible" systems and the persistence of the metastable small-H local free energy minimum for the "exfoliated" systems—appear to be universal and robust, at least within the parameter space investigated here.

What are the practical implications of this new model? First, it suggests that intercalated morphologies should be observed, indeed, for the majority of nanocomposites. In fact, it is likely that in the melt almost all nanocomposites exhibit gallery expansion compared to the room-temperature organoclays (see, e.g., Vaia et al.[30,31]). As nanocomposite is cooled down from the melt to room temperature, the average gallery spacing could shrink back or stay expanded, depending on various kinetic factors. Second, it suggests caution in assuming that intercalated structures must lead to physical or mechanical property improvements. If intercalation proceeds because of the "frozen" density reduction in the galleries, rather than because of the true incorporation of the matrix polymer, the interface between clay and polymer will remain weak, and it would likely adversely impact properties such as toughness. Finally, it is important to note that even for the supposedly exfoliated nanocomposites, the presence of a local free energy minimum means that there is a strong barrier to exfoliation.[32] As discussed by Ginzburg, Gendelman, and Manevitch,[33−35] if the free energy profile has a double-well structure, the transition from intercalated to exfoliated morphology takes place only when a sufficiently strong shear force is applied to overcome the barrier. The transition would occur via a so-called "kink" mechanism, and the kink could appear if—and only if—the clay stack is subjected to shear stresses on the order of 1 GPa.[36] Thus, it is easy to understand why—even if thermodynamically the nanocomposite should be exfoliated—large fraction of the clay platelets still remain in the metastable, intercalated state.

Yet another implication of the model—and a potentially testable prediction—is that, all other things being equal, one could find a higher degree of intercalation in nanocomposites with lower density matrix polymers, compared to ones with higher density. We are not aware of experimental studies directly testing this proposition (although studies by Vaia and coworkers[30,31] appear to provide indirect evidence, as discussed above); we hope that our theoretical analysis would stimulate new investigation in this direction.

Conclusions

We applied a "compressible" lattice self-consistent field theory (SCFT) to study the phase behavior of polymer−clay nanocomposites. Specifically, we chose a system in which organically modified clay was added to a mixture of homopolymers and "one-sticker" active chains. The predictions of the "compressible SCFT" were compared to the incompressible SCFT modeling results similar to those of Balazs et al.[6−10] It was found that accounting for the polymer compressibility leads to two important effects:

- In the phase map region where no exfoliation is expected (concentration of active functional groups is too low or their adhesion to clay is too weak), there still could be "intercalation" due to the equilibration of the densities in the gallery and in the bulk. If this increased gallery height could be preserved upon cooling, the material would be considered "intercalated" since the average interparticle distance (d_{001} peak in the wide-angle X-ray scattering) is higher than in the pristine organoclay. (It is possible that this is the nature of the effect observed recently by Swain and Isayev.[24])
- In the phase map region where exfoliation is expected (strong adhesion between clay and "stickers"), the above-mentioned intercalated free energy minimum is still present and must be compared to the "exfoliated" state. In particular, in the region where the adhesion is "strong" but "not strong enough", the compressible model predicts intercalated morphology even as the incompressible model anticipated exfoliated structures.

We anticipate that these findings probably could be applied to other types of melt-compounded nanocomposites. Certainly, polymer-mediated thermodynamic analysis does not provide a full description of the nanocomposite physics, as the morphology of the system is strongly influenced by clay−clay electrostatic and van der Waals interactions, excluded volume interactions and rheology (especially at higher clay loadings), thermal and shear history, and other factors. However, it suggests an interesting mechanism of understanding the factors responsible for the development of intercalated morphologies. In particular, our model suggests that there is a strong relationship between polymer density and the nature of intercalated composites. We intend to study this relationship in our future work.

Acknowledgment. We thank The Dow Chemical Company for the support of this research. We are grateful to Dr. YuanQiao Rao (Dow), Prof. Walter Chapman (Rice University),

Dr. Richard Vaia (AFRL), Prof. Alexander Patashinski (Northwestern University), and Prof. Anna Balazs (University of Pittsburgh) for stimulating discussions. Finally, we thank anonymous reviewers for helpful comments and suggestions.

References and Notes

(1) Okada, A.; Kawasumi, M.; Usuki, A.; Kojima, Y.; Kurauchi, T.; Kamigaito, O. Synthesis and properties of nylon-6/clay hybrids. In Schaefer, D. W., Mark, J. E., Eds.; *Polymer Based Molecular Composites*; MRS Symposium Proceedings, Pittsburgh, 1990; Vol. *171*, pp 45−50.

(2) Sinha Ray, S.; Okamoto, M. *Prog. Polym. Sci.* **2003**, *28*, 1539, and references therein.

(3) Alexandre, M.; Dubois, P. *Mater. Sci. Eng. R* **2000**, *28*, 1, and references therein.

(4) Vaia, R. A.; Giannelis, E. P. *Macromolecules* **1997**, *30*, 7990.

(5) Vaia, R. A.; Giannelis, E. P. *Macromolecules* **1997**, *30*, 8000.

(6) Balazs, A. C.; Singh, C.; Zhulina, E. *Macromolecules* **1998**, *31*, 8370.

(7) Zhulina, E.; Singh, C.; Balazs, A. C. *Langmuir* **1999**, *15*, 3935.

(8) Balazs, A. C.; Singh, C.; Zhulina, E.; Lyatskaya, Y. *Acc. Chem. Res.* **1999**, *32*, 651.

(9) Ginzburg, V. V.; Singh, C.; Balazs, A. C. *Macromolecules* **2000**, *33*, 1089.

(10) Ginzburg, V. V.; Balazs, A. C. *Adv. Mater.* **2000**, *12*, 1805.

(11) Kuznetsov, D.; Balazs, A. C. *J. Chem. Phys.* **2000**, *112*, 4365.

(12) Kuznetsov, D.; Balazs, A. C. *J. Chem. Phys.* **2000**, *113*, 2479.

(13) Fleer, G. J.; Cohen Stuart, M. A.; Scheutjens, J. M. H. M.; Cosgrove, T.; Vincent, B. *Polymers at Interfaces*; Chapman & Hall: London, 1993.

(14) Scheutjens, J. M. H. M.; Fleer, G. J. *J. Phys. Chem.* **1979**, *83*, 1619.

(15) Scheutjens, J. M. H. M.; Fleer, G. J. *J. Phys. Chem.* **1980**, *84*, 178.

(16) Lyatskaya, Y.; Balazs, A. C. *Macromolecules* **1998**, *31*, 6676.

(17) Balazs, A. C.; Ginzburg, V. V.; Lyatskaya, Y.; Singh, C.; Zhulina, E. Modeling the Phase Behavior of Polymer-Clay Nanocomposites. In *Polymer-Clay Nanocomposites*; Pinnavaia, T., Beall, G., Eds.; Wiley: New York, 2000.

(18) Beyer, F. L.; Beck Tan, N. C.; Dasgupta, A.; Galvin, M. E. *Chem. Mater.* **2002**, *14*, 2983.

(19) Kurian, M.; Beyer, F. L.; Dasgupta, A.; Galvin, M. E. *J. Polym. Sci., Part B: Polym. Phys.* **2004**, *42*, 4075.

(20) Garces, J. M.; Moll, D. J.; Bicerano, J.; Fibiger, R. F.; McLeod, D. G. *Adv. Mater.* **2000**, *12*, 1835.

(21) Hasegawa, N.; Okamoto, H.; Kawasumi, M.; Kato, M.; Tsukigase, A.; Usuki, A. *Macromol. Mater. Eng.* **2000**, *280/281*, 76.

(22) Wang, K. H.; Choi, M. H.; Koo, C. M.; Choi, Y. S.; Chung, I. J. *Polymer* **2001**, *42*, 9818.

(23) Koo, C. M.; Kim, S. O.; Chung, I. J. *Macromolecules* **2003**, *36*, 2748.

(24) Swain, S. K.; Isayev, A. I. *Polymer* **2007**, *48*, 281.

(25) Jain, S.; Jog, P.; Ginzburg, V. V.; Srivastava, R.; Weinhold, J. D.; Chapman, W. G. *J. Chem. Phys.* **2009**, *131*, 044908.

(26) van Lent, B.; Israels, R.; Scheutjens, J. M. H. M.; Fleer, G. J. *J. Colloid Interface Sci.* **1990**, *137*, 380.

(27) The interaction parameter between hydrocarbon polymer and "voids", χ_{pv}, could be estimated based on the known surface tension of polyethylene (see, e.g., ref 28), $\chi_{pv} \simeq (v_{ref}/a)(\gamma/k_BT)$, where $\gamma \approx 25-35$ mN/m is the surface tension of polyethylene, $v_{ref} \sim 0.05-0.1$ nm^3 is the "reference" monomer volume, $a = 0.4$ nm is the lattice unit length, $k_B = 1.38 \times 10^{-23}$ J/K is Boltzmann's constant, and T is absolute temperature. Thus, we obtain $\chi_{pv} \sim 1.0$—2.0 and choose $\chi_{pv} = 1.0$ for this study.

(28) Bicerano, J. *Prediction of Polymer Properties*, 3rd ed.; Marcel Dekker: New York, 2002; Chapter 7.

(29) Cao, D.; Wu, J. *Langmuir* **2006**, *22*, 2712.

(30) Vaia, R. A.; Teukolsky, R. K.; Giannelis, E. P. *Chem. Mater.* **1994**, *6*, 1017.

(31) Jacobs, J. D.; Koerner, H.; Heinz, H.; Farmer, B. L.; Mirau, P.; Garrett, P. H.; Vaia, R. A. *J. Phys. Chem. B* **2006**, *110*, 20143.

(32) To better illustrate the significance of the polymer-induced barriers between intercalated and exfoliated states, we consider the example shown in Figure 4a. The free energy units are in terms of "kT/lattice unit area"; one lattice unit area is $\sim a^2 \sim 0.2$ nm^2. Thus, intercalation barrier of Figure 4a would correspond to about 0.01 kT/0.2 nm$^2 \sim 0.05$ kT/nm^2. For a montmorillonite platelet with diameter $D \sim 200$ nm, the total area per platelet is $\sim \pi D^2/4 \sim 31\,000$ nm^2. Hence, the total strength of the attraction between the two platelets is on the order of 1500 kT, or about 750 kcal/mol.

(33) Ginzburg, V. V.; Gendelman, O. V.; Manevitch, L. I. *Phys. Rev. Lett.* **2001**, *86*, 5073.

(34) Gendelman, O. V.; Manevitch, L. I.; Manevitch, O. L. *J. Chem. Phys.* **2003**, *119*, 1066.

(35) Balazs, A. C.; Bicerano, J.; Ginzburg, V. V. Polyolefin/Clay Nanocomposites: Theory and Simulation. In *Polyolefin Composites*; Nwabunma, D., Kyu, T., Eds.; Wiley: New York, 2008.

(36) The "kink" model stipulates that the penetration of polymer into the gallery is not instantaneous but is limited by a slow propagation of a "bending kink" along one of the two adjacent clay platelets. According to that analysis, a kink would propagate with nonzero speed only when there is a shear stress, τ, in excess of a threshold stress $\tau^* = (AEI)^{1/2}/(U_0\delta)$. Here, $A \sim 0.1$ kT/nm$^2 \sim 0.05$ J/m^2 is the second derivative of the free energy with respect to plate separation; $E \sim 100$ GPa is the Young's modulus of the platelet; $\delta \sim 1$ nm is the platelet thickness; $I = \delta^3/12$; and $U_0 \sim 1$ nm is the gallery height prior to polymer intercalation. Thus, $\tau^* \sim 1$ GPa. For more details, see refs 33−35.